# Solar Radiation Mapping from NOAA AVHRR Data in Catalonia, Spain

HENRY FLORES TOVAR AND JOSE M. BALDASANO

*Departamento de Proyectos de Ingeniería, Universidad Politécnica de Cataluña, Barcelona, Spain*

(Manuscript received 13 November 2000, in final form 23 April 2001)

ABSTRACT

A statistical model is presented for the determination of hourly global solar radiation from the National Oceanic and Atmospheric Administration advanced very high resolution radiometer (NOAA AVHRR) satellite data, which provide wide coverage together with adequate spatial resolution (around 1.1 km at the nadir). The process is divided into three steps. The first step consists of a cloud detection procedure. The second step determines the cloud index for each point on the satellite image, which is then used for the third step, which is the application of the global solar radiation statistical model. The coefficients for the model are determined by regression from the data obtained from 11 global surface solar radiation measurement stations (pyranometers). Once the coefficients have been determined, a surface interpolation is performed to obtain the entire coefficient field for the area under study, with the objective of applying the model. The estimates obtained from the model were compared with data from another 10 ground radiation measurement stations in Catalonia, Spain. This model was tested for the 11 consecutive months beginning in February of 1998, with an excellent correlation being obtained between the estimate provided by the model and the data from the measurement stations, which resulted in a coefficient of determination of greater than 0.98 in all cases, together with an rmse of between 9.6% and 15.8% and a bias that varied from 9.5% to 1.3%. In southern Catalonia, satellite-estimated and surface-interpolated hourly global solar radiation were of equal quality (rmse of about 3%–15%). In northern Catalonia, where the stations are more sparse, the satellite-estimated values were more accurate (rmse of 7%) than those obtained from interpolation of surface station data (rmse of 11%–16%).

## 1. Introduction

The use of satellite data to estimate solar irradiance at ground level represents a valid alternative to ground measurements of solar radiation. A number of articles have been published on this issue, developing different methodologies for this purpose and using different kinds of images from different satellites.

In the review paper by Noia et al. (1993), the best-known models for estimating the solar irradiance at the earth's surface using geostationary satellite data were presented. Recently, Pinker et al. (1995) presented an update of the methods to derive shortwave radiation from satellite observation since the early 1990s, along with a summary of the current status and availability of global datasets of downward surface shortwave radiation.

The models employed to estimate global surface solar radiation from satellite data can essentially be divided into two categories: statistical (or empirical), which consist of establishing a relationship between the satellite data and the measurements made on the surface, and physical (or theoretical), which make use of radiative transfer models to relate the satellite data with the surface measurements.

There are many factors that make this estimation of global solar radiation via satellite data a difficult task. Clouds are the first-order solar radiation attenuators, and atmospheric constituents (aerosols, water vapor, and other gaseous molecules) are the second-order attenuators (Tarpley 1979).

The detection of the presence of clouds is important when attempting to obtain precise estimates of global surface solar radiation, and it is for this reason that this study uses a cloud detection algorithm that is based on the definition of thresholds in the various National Oceanic and Atmospheric Administration (NOAA) satellite reception channels, thus constituting a multispectral detection technique (Karlsson 1989; Allen et al. 1990; Laine et al. 1999).

Through the use of regression techniques, Tarpley (1979) estimated daily insolation with data from Geostationary Operational Environmental Satellites (GOES) and pyranometer measurements over the Great Plains of the United States. The standard error in the satellite estimate produced by Tarpley as compared with the one measured over the surface was less than 10% of the average daily insolation and less than 5% for clear days, with a correlation of 0.90.

*Corresponding author address:* Jose M. Baldasano, Dept. Proyectos de Ingeniería, ETSE1B-UPC, Av. Diagonal 647, 10.23, 08028 Barcelona, Spain.
E-mail: baldasano@pe.upc.es

Gautier et al. (1980) presented a simple physical model for the determination of incident surface solar radiation using GOES satellite data in the southeast of Canada. The standard error in the daily estimate on clear days was less than 5% of the average. This same index was around 14%–15% on completely overcast days, and, for all combined cases, it was less than 9%.

Cano et al. (1986) presented a statistical model for the determination of global surface solar radiation from the Meteosat meteorological satellite. The statistical results of comparing the satellite estimate and the hourly global solar radiation measured on the surface, using the data from 27 measurement stations belonging to the French Meteorological Office, showed an average correlation factor of 0.87 with a root-mean-square error (rmse) of 42.2 J $cm^{-2}$.

Nunez (1987) applied a linear model to the determination of global daily solar radiation in Tasmania, Australia, from the visible channel of geostationary meteorological satellite images and from the records of three solar radiation measuring stations on the surface, obtaining an error of less than 13% in the satellite estimate of the daily mean global solar radiation as measured in situ.

Rafiqul et al. (1996) presented a bispectral empirical model with application in the visible and infrared image bands from satellites belonging to NOAA for determining and drawing daily global solar radiation maps in south and southeast Asia. The standard error in the estimation of the daily global solar radiation was 12%, with a variability range of between 6% and 19% of the measured mean value.

Bishop et al. (1997) presented an 8-yr (July 1983–June 1991) time series of daily and monthly mean surface solar irradiance produced for the globe. The long time series is derived from the cloud radiative properties retrieved by the International Satellite Cloud Climatology Project from radiances measured by four geostationary and two polar-orbiting weather satellites.

Laine et al. (1999) applied a physical model for the estimation of instantaneous global solar radiation and the accumulated daily insolation in Finland from data collected by the NOAA satellite advanced very high resolution radiometer (AVHRR). The standard-error variability range of instantaneous global solar irradiation in cloudy conditions was between 17% and 39%, but the standard error of daily cumulative insolation was less than 7% in clear cases and varied between 11% and 19% in cloudy cases.

The methodology employed in this work is of a statistical approach. The data from ground measurement stations are used to determine the regression coefficients of the model, which are then used to determine the total radiation. The basic idea of the model is that the amount of cloud covering a specific area will statistically determine the global solar radiation received by this area. The first step consists of a multispectral cloud detection procedure. The second step determines the cloud-cover index for each point on the image ($i$, $j$), called a pixel, which is then used in the third step for the statistical determination of the global solar radiation model.

This procedure was applied in Catalonia, which is located in the northeastern corner of Spain and is limited by the Mediterranean Sea and by the Pyrenean Mountain range to the north. The Catalonia territory is roughly triangular in shape, with an area of 31 895 $km^2$ (Fig. 1).

A similar methodology has been widely employed by the Agence Française pour la Maîtrise de l'Energie (Diabaté et al. 1989) and by the European Solar Radiation Atlas (Beyer et al. 1997; Kasten et al. 1996) for the production of solar radiation maps of the European continent by application of the Heliosat method. The Heliosat method, as developed by Diabaté et al. (1989), produces solar radiation maps with adequate temporal (hourly) and spatial scales (on the order of 1 pixel size of 5 km $\times$ 5 km of the Meteosat image), such as those obtained by Cano et al. (1986).

The main difference between the methodology described in this contribution and that developed by Heliosat has to do with the determination of monthly regression coefficients. In our model, regression coefficients are determined on a monthly basis, accounting for spatial and seasonal variations. Heliosat methodology, however, only considered a single set of regression coefficients per hour, which are constant throughout the year and in space.

## 2. Method

### *a. Total atmospheric transmission factor*

The total atmospheric transmission factor $K(i, j)$ is defined as the ratio of the solar radiation reaching the ground through an atmospheric column $G(i, j)$ to the extraterrestrial solar radiation incident at the top of the column $G_o(i, j)$:

$$K(i, j) = G(i, j)/G_o(i, j). \tag{1}$$

### *b. The cloud-cover index for the satellite images*

Cloudiness is expressed through the cloud-cover index $n^t(i, j)$ at a given point $(i, j)$ and a given time $t$ by applying the following formula (Cano et al. 1986):

$$n^t(i, j) = \frac{[\alpha^t_{\text{toa}}(i, j) - \alpha_{\text{toa,min}}(i, j)]}{[\alpha_{\text{toa,max}}(i, j) - \alpha_{\text{toa,min}}(i, j)]}, \tag{2}$$

where $\alpha^t_{\text{toa}}(i, j)$ is the instantaneous planetary albedo; $\alpha_{\text{toa,min}}(i, j)$ corresponds to a clear, clean, and dry sky; and $\alpha_{\text{toa,max}}(i, j)$ corresponds to a heavily overcast sky.

The existence of clouds, from the sensor point of view, is translated into an increase in the planetary albedo. The cloud-cover index varied from 0 to 1 and may be interpreted as the cloud coverage percentage per pixel. In addition, it is an indicator of the atmospheric

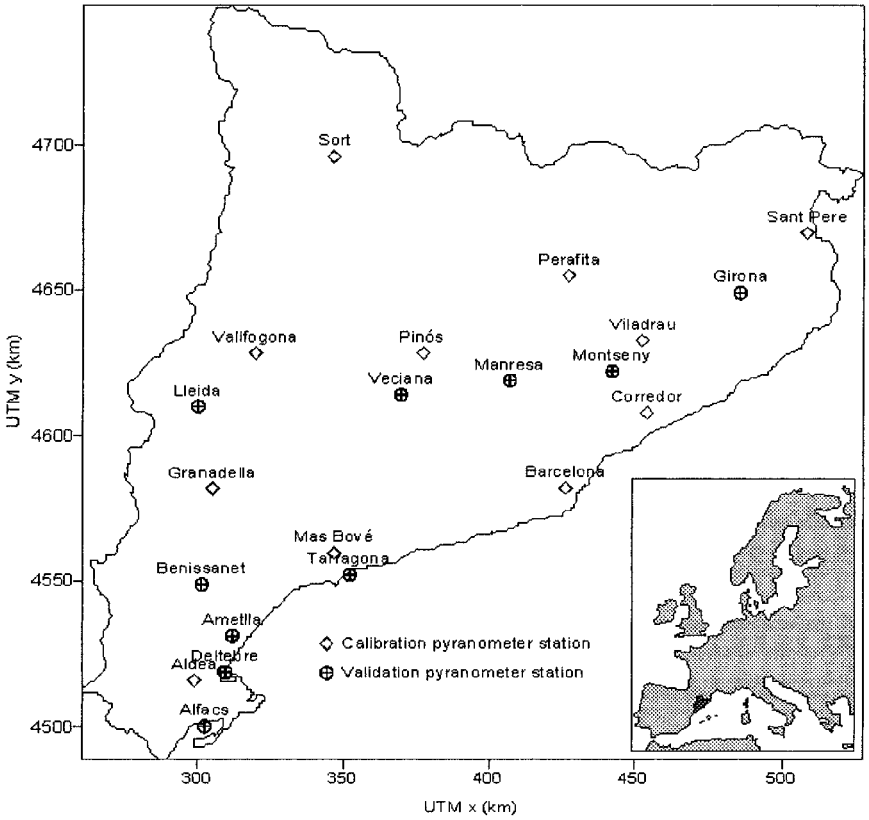


FIG. 1. The location of Catalonia within Europe, and ground measurement stations.

transmission of a column of air located above the pixel, where low values correspond to a high factor of atmospheric transmission.

### *c. Statistical relationship between the atmospheric transmission factor and the cloud-cover index*

The method consists of assuming a linear regression between the atmospheric transmission factor and the cloud-cover index determined by the satellite images in the following way:

$$K^t(i, j) = a(i, j)n^t(i, j) + b(i, j), \quad (3)$$

where coefficient $a$ corresponds to the slope of the curve and $b$ represents the atmospheric transmission with a clear sky, which is a more stable coefficient than $a$, which is extremely influenced by cloudiness conditions. The coefficients $a$ and $b$ are assumed to be constant for a period of 1 month for each point of the surface.

The regression coefficients can be determined by comparing the transmission factors deduced from the solar radiation data measured at ground level with the corresponding cloud-cover index derived from satellite images. Once these coefficients are known at ground stations, methods of interpolation may be applied to define the complete field of coefficients for the study area.

In agreement with the general knowledge of solar radiation, this relationship is restricted to solar elevations greater than 12° and to satellite elevations greater than 5°. It follows that this method cannot operate optimally for latitudes greater than about 60° (Diabaté et al. 1989).

An expression having the same form as that of Eq. (3) was employed by Cano et al. (1986), Nunez (1987), Diabaté et al. (1989), and Rafiqul et al. (1996). Cano et al. (1986) used images from the Meteosat satellite to determine the cloud-cover index; Nunez (1987) only made use of the planetary reflectivity; Diabaté et al. (1989) used the visible channel of geostationary satellite images to obtain global solar radiation maps employing the Heliosat method, which was verified during 30 consecutive months beginning in January of 1983; Rafiqul et al. (1996) employed a bispectral method with application in the visible and thermal infrared ranges of NOAA images to calculate the sky's cloud cover.

## 3. Operational procedure

### *a. Data collection and filtering from the ground measurement stations*

Data were collected from 30 global solar radiation surface measurement stations that belong to the net-

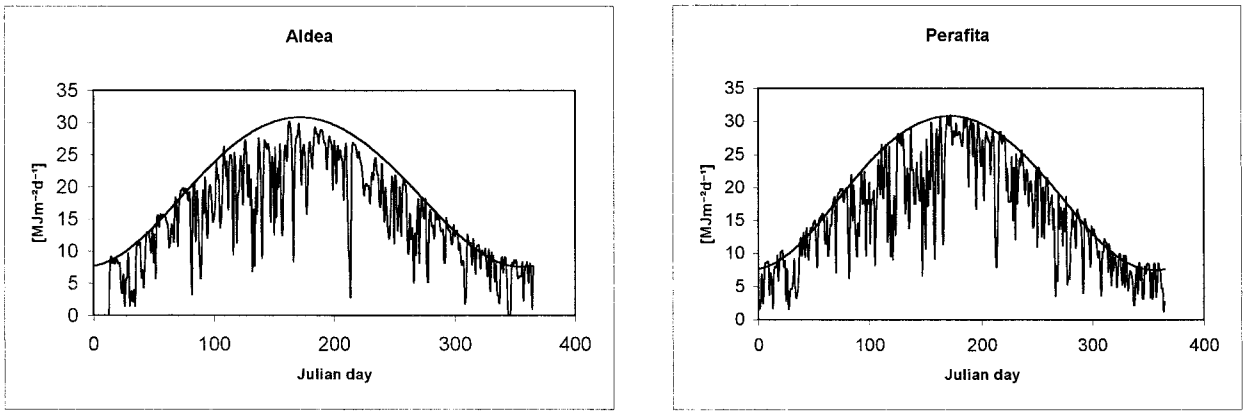


FIG. 2. An example of the filtering process for temporal coherence of the data from the ground measurement stations. The smooth line represents the daily irradiation analytic curve, and the other line corresponds to the data from the stations.

works of the Spanish National Institute of Meteorology (INM), Institut Català d'Energia (ICAEN), and the Department d'Agricultura Ramaderia i Pesca (DARP), each a part of the agrimeteorological network of the Generalitat of Catalonia, which is distributed throughout Catalonia. The measurements were performed using Kipp & Zonen, Inc., Siap, Inc., and Campbell Scientific, Inc., pyranometers. The dataset consisted of 5-min averages of irradiance, together with the daily cumulative insolation for 1998.

These measurement stations are not homogeneously distributed within the territory because their locations depend on a range of factors. Station density is high along the coast and in the central region of Catalonia but is more sparse as one moves closer to the mountains in the north.

A careful filtering process is applied to the pyranometer data to correct any possible measurement errors, for example, flat sensors, the presence of shade, poor calibration, and so on. This process is particularly relevant to this study because any error in the measurements may lead to enormous spatial variability in the data. The method consists of the analysis of a series of data based on two criteria: temporal and spatial coherence of the data.

Temporal coherence is checked by means of a series of graphs, one for each station. An example of these graphs is shown in Fig. 2, which provides data from the Aldea and Perafita stations. Note that the analytic curve has been drawn together with the data series on this figure. This curve was analytically generated by taking into account only the astronomical evolution of daily radiation (for a given latitude and air transmittance) and provides an estimate of the solar radiation at sea level under clear-sky conditions. This curve is employed as a reference to check the evolution of clear days throughout the year. Considerable deviation of the measurements with respect to this curve (not justified by the characteristics of the measurement station site: located on top of a mountain or in misty atmospheric conditions, for example) indicates possible measurements errors. For example, a seasonal deviation could be an indication of the presence of shade at the measurement station site. If the measurements are consistently above or below the curve, then the sensor could be out of calibration.

The spatial coherence of the data is studied simultaneously using a series of radiation isoline maps with global solar radiation maps for Catalonia reported by Santabárbara et al. (1996) and Baldasano et al. (1999), taking into account the fact that stations that are close together should not provide very different records. Some of the sensors were calibrated to obtain various points of control that were used as references during this process.

After combining the two coherence criteria, some of the data periods were eliminated. In some cases, the total data for a particular station were eliminated. This led to the elimination of 9 of the initial 30 stations. The locations of the stations that passed the filtering process are shown in Fig. 1.

### *b. Satellite data*

This study makes use of data obtained from the polar-orbiting satellite NOAA AVHRR. The spatial resolution of these images is 1.1 km at nadir. The spectral bands (wavelengths in micrometers) of the AVHRR sensor, from channel 1 to channel 5, are, respectively, 0.58–0.68, 0.72–1.10, 3.55–3.93, 10.3–11.3, and 11.5–12.5.

Work was carried out with 189 images for 1998 (see Table 1), which were captured by the receiving station belonging to the Environment Department of the Generalitat of Catalonia, using a Dartcom, Ltd., high-resolution picture transmission system receiver. These images come in an 8-bit format that is geometrically corrected and duly georeferenced.

For temporal resolution, two images may be obtained daily at approximately 0730 and 1430 LST, which correspond to the pass of the morning satellite (*NOAA-15*) and the afternoon satellite (*NOAA-14*) respectively.

TABLE 1. NOAA images from 1998.

| Month | Days |
|---|---|
| Jan | — |
| Feb | 14 |
| Mar | 18 |
| Apr | 13 |
| May | 14 |
| Jun | 21 |
| Jul | 29 |
| Aug | 21 |
| Sep | 20 |
| Oct | 18 |
| Nov | 14 |
| Dec | 7 |
| Total | 189 |

However, for technical reasons, in this study only the images corresponding to 1430 LST (*NOAA-14*) were available. The image header provides information about the satellite, date and time of acquisition, receiver channel (band), and the calibration coefficients. Image calibration is linear. When it belongs to the visible channel, it provides the albedo; if it is within the thermal infrared band, it provides information about the temperature.

### c. Cloud detection

In general terms, cloud detection using satellite images depends on the contrast between the clouds and the background. In the visible band, this contrast is examined in terms of reflection levels. In infrared, we observe brightness temperature difference, which includes both the effects of reflection levels and thermal emission.

A simple, fast technique for cloud detection consist of the evaluation of radiance, together with the application of predetermined thresholds between various channels of the AVHRR sensor, which enables the various types of surface (land, sea, snow, etc.) and cloud to be discriminated. Allen et al. (1990) and Laine et al. (1999) developed and evaluated algorithms for discriminating among clouds, snow, and land surfaces employing a multispectral technique on channels 1, 3, and 4 of the NOAA AVHRR sensor.

In this work, cloud detection was carried out using the algorithm developed by Laine et al. (1999), which uses the mean reflection level of channel 1 ($R_1$) together with the brightness temperature from channels 3 and 4 ($T_3$ and $T_4$, respectively) to enable the separation of clouds, snow, and land, with the procedure basically consisting of four tests. The first test assumes that clouds are usually cooler than the land, except under conditions of atmospheric thermal inversion. By taking advantage of this condition, the cold clouds located in the high atmospheric layers may be identified by applying a minimum value of brightness temperature ($T_{\min}$) for channel 4. The second test consists of a general procedure for cloud detection, by means of the application of an empirical threshold of 8 K for $T_3 - T_4$, which permits clouds to be separated with respect to the land and the sea. The third test enables the high reflection level of clouds and snow to be separated from areas that are snow-free land by the application of a minimum reflection level of 0.15 for channel 1. The final test separates the clouds from snow and ice, using the same principle as test 2 but with an empirical threshold of 4 K.

### d. Determining the hourly global solar radiation from satellite data

From the 21 available measurement stations described in section 3a, only 11 were selected for determining the *a* and *b* coefficients (calibration stations) of the atmospheric transmission factor equation. The remaining 10 measurement stations were used for model validation (see Table 2). For each one of the calibration stations, the atmospheric transmission factor is calculated by application of Eq. (1).

For satellite images, the procedure consists of working with a set of images: in this case, all daytime images for a month. The visible and infrared image channels are used to detect the clouds, and the visible channel is used to determine the albedo of both the surface and the clouds.

Each visible image is normalized by dividing by the cosine of the local solar zenith angle. The cloud-cover index is determined by applying a statistical procedure that takes into account the possibility of a pixel being contaminated with clouds or not being contaminated. All daytime images for the month under analysis are taken, and the minimum value for each pixel is taken, giving information on the clear-sky planetary albedo for every pixel ($\alpha_{\text{toa,min}}$). In a similar way, the maximum value for each pixel in the series is also determined, which corresponds to the planetary albedo of the overcast cloudy sky including cloud top and the atmosphere above the cloud ($\alpha_{\text{toa,max}}$). Then the cloud index is determined for each pixel by application of Eq. (2).

Coefficients *a* and *b* are determined from field data, defining a linear regression [Eq. (3)] between the transmission factor deduced from the solar radiation data measured at ground and the cloud-cover index at the same location determined from satellite. For example, in Fig. 3 a scatterplot of atmospheric transmission factor versus cloud-cover index is shown for 1998 for stations Aldea and Perafita. The yearly regression equation is also included.

Table 3 shows the monthly value obtained for the *a* and *b* coefficients, together with the determination coefficient $r^2$, for the Aldea and Perafita stations. Note that a determination coefficient $r^2 \approx 0.80$ was obtained for the mean values for all the stations, so that the obtained values of the model coefficients by regression represent a good fit.

After determining the model coefficients, the varia-

TABLE 2. Ground measurement stations.

| No. | Station | UTM *x* (km) | UTM *y* (km) | *z* (m) | Apparatus type | Source |
|---|---|---|---|---|---|---|
| | | | Stations used for model calibration | | | |
| 1 | Aldea | 298.910 | 4516.110 | 62 | Campbell | DARP |
| 2 | Barcelona | 426.140 | 4581.770 | 99 | Kipp & Zonen | ICAEN |
| 3 | Corredor | 453.870 | 4607.930 | 459 | Campbell | DARP |
| 4 | Granadella | 305.000 | 4581.550 | 490 | Campbell | DARP |
| 5 | Mas Bové | 346.575 | 4559.500 | 105 | Campbell | DARP |
| 6 | Perafita | 427.207 | 4654.918 | 770 | Campbell | DARP |
| 7 | Pinós | 377.232 | 4628.436 | 650 | Campbell | DARP |
| 8 | Sant Pere | 508.000 | 4669.600 | 5 | Campbell | DARP |
| 9 | Sort | 346.370 | 4695.960 | 700 | Kipp & Zonen | ICAEN |
| 10 | Vallfogona | 319.600 | 4628.320 | 245 | Campbell | DARP |
| 11 | Viladrau | 452.400 | 4632.648 | 860 | Campbell | DARP |
| | | | Stations used for model validation | | | |
| 12 | Alfacs | 302.380 | 4500.160 | 0.5 | Campbell | DARP |
| 13 | Ametlla | 311.805 | 4531.280 | 95 | Kipp & Zonnen | ICAEN |
| 14 | Benissanet | 301.350 | 4548.625 | 30 | Campbell | DARP |
| 15 | Deltebre | 309.550 | 4518.850 | 1.5 | Campbell | DARP |
| 16 | Girona | 485.450 | 4649.010 | 100 | Kipp & Zonnen | ICAEN |
| 17 | Lleida | 300.030 | 4610.080 | 199 | Siap | INM |
| 18 | Manresa | 407.106 | 4619.002 | 250 | Kipp & Zonnen | ICAEN |
| 19 | Montseny | 442.120 | 4622.198 | 990 | Campbell | DARP |
| 20 | Tarragona | 352.000 | 4552.000 | 20 | Kipp & Zonnen | ICAEN |
| 21 | Veciana | 369.570 | 4614.035 | 725 | Campbell | ICAEN |

tion over time and space can be clearly observed (including seasonal variations) so that it is sufficient to calculate them on a monthly basis and assume they are constant throughout the considered month (Rafiqul et al. 1996). This point of the method is different from Cano et al. (1986), who considered the coefficients to be constant with time, with only a slight seasonal variation, or Diabaté et al. (1989), who considered that the model coefficients were constant for a given hour of the day, both in time and space, throughout the year.

Once these coefficients were known at the ground stations, an interpolation process (kriging method) was performed to obtain the *a* and *b* field of the area under study. Hourly global solar radiation was then determined for the whole study area using the procedure shown in Fig. 4.

## 4. Discussion of the results

### *a. Cloud detection algorithm*

Figure 5 shows the application of the cloud detection algorithm for a NOAA image acquired on 11 August 1998. In this figure, bands 1, 3, and 4 of the AVHRR sensor are represented, which correspond to albedo (%) and the brightness temperature (K) for bands 3 and 4, respectively.

When test 1 is applied, high clouds (cirrus, cirrocu-

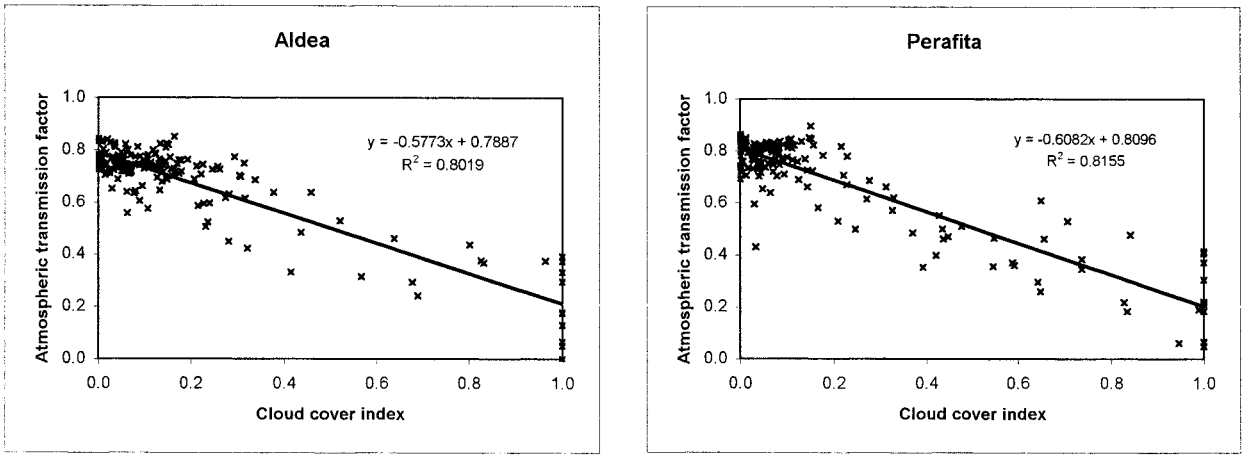


FIG. 3. Example of linear regression between the satellite cloud-cover index and pyranometer-measured transmission factor for the Aldea and Perafita stations for 1998.

TABLE 3. Model coefficient ($a$, $b$) and determination coefficient ($r^2$) values.

| | Aldea | | | Perafita | | |
|---|---|---|---|---|---|---|
| Month | $a$ | $b$ | $r^2$ | $a$ | $b$ | $r^2$ |
| Feb | −0.4838 | 0.8189 | 0.8750 | −0.4350 | 0.8394 | 0.8769 |
| Mar | −0.6518 | 0.8305 | 0.8730 | −0.7152 | 0.8734 | 0.9455 |
| Apr | −0.5412 | 0.8391 | 0.9018 | −0.7422 | 0.8589 | 0.9362 |
| May | −0.7228 | 0.7620 | 0.9805 | −0.6776 | 0.8128 | 0.9415 |
| Jun | −0.3730 | 0.7645 | 0.8928 | −0.7782 | 0.8370 | 0.9664 |
| Jul | −0.5249 | 0.7978 | 0.8794 | −0.5244 | 0.8205 | 0.8076 |
| Aug | −0.6545 | 0.7610 | 0.8854 | −0.5807 | 0.7476 | 0.7062 |
| Sep | −0.6268 | 0.7344 | 0.8230 | −0.5616 | 0.8062 | 0.7775 |
| Oct | −0.3587 | 0.7906 | 0.8012 | −0.6864 | 0.7821 | 0.7975 |
| Nov | −0.7171 | 0.7699 | 0.9029 | −0.3455 | 0.7261 | 0.7589 |
| Dec | −0.7591 | 0.7901 | 0.9570 | −0.5103 | 0.7399 | 0.9767 |
| Annual | −0.5773 | 0.7887 | 0.8019 | −0.6082 | 0.8096 | 0.8155 |

mulus, etc.) are more evident and appear at the Pyrenean Mountain range and the upper part of the image. When test 2 is applied, some middle clouds appear (altocumulus, altostratus, etc.) both in the Gulf of Vizcaya and the Gulf of Lyon and over the Mediterranean Sea. When test 3 is applied, high and middle clouds appear again together with low clouds (cumulus, stratus, etc.). These clouds are located over a great continental extension toward the lower-left corner of the image. Test 4 detects a series of low clouds located at Gulf of Lyon, at the Mediterranean Sea, and the Balearic Islands, which were not detected in the previous tests. In the last image, all clouds types are represented. To obtain a detailed cloud classification, the procedure described by Karlsson (1989) can be applied.

According to a visual check of the efficiency for the separation of clouds and snow, values close to 100% were obtained under snow-free conditions, just like the values reported by Laine et al. (1999) under similar circumstances.

The employed cloud detection algorithm was good at effectively discriminating the clouds from the land, snow, and ice. Note that, in the study area, the northern-central Catalonia (during certain short periods of time in winter) and the Pyrenean Mountain range (during the whole winter period) may reveal wide areas covered in snow, so that most of the test-3 cases described in section 3c are sufficient for adequate cloud detection.

### *b. Comparison of satellite-estimated, surface pyranometer-interpolated, and pyranometer-measured hourly global solar radiation*

To validate the satellite estimates of hourly global solar radiation, two comparisons were carried out. First, comparisons were made of satellite estimates with ground pyranometer data. A second comparison was conducted among satellite estimates, surface pyranometer-interpolated data, and ground pyranometer measurements. Both for satellite-estimated and for surface pyranometer-interpolated data, measurements from the calibration stations were used. The result obtained were later compared with another set of independent stations (validation stations).

Figure 6 shows a comparison between the hourly global solar radiation as estimated by satellite and that obtained by measurement stations on the ground for the period of January–December 1998. The diagonal line of slope 1 shows a perfect fit between the estimate by satellite and the measurements, whereas the dotted line represents the curve adjusted by regression of the values. Equations in each plot represent the regression coefficients of the best-fitted line adjusted for each dataset. The determination coefficient for each case is also included. Table 4 shows the values of the comparison between the hourly global solar radiation as estimated by satellite and that measured by the pyranometers, showing the mean, the rmse, and the bias for each of the model validation stations. The results show a determination coefficient of $r^2 > 0.98$ in all cases, together with a minimum rmse of 9.6% and a bias of −0.8% for the Deltebre station, whereas a maximum bias of −9.5% with an rmse of 15.7% is obtained for the Lleida station, so that the fit is very good. Only in a few stations, such as Ametlla, Lleida, and Girona, can it be seen that the model slightly underestimates the radiation value given by the pyranometers. For the remaining stations, it can be said that the model correctly estimates the measurements, providing estimated values that are very close to the measured value. Only in the Manresa station is a positive bias value of 1.3% obtained, with an rmse of 10.0%.

The ultimate test for satellite estimates of hourly global solar radiation is to compare them with the surface pyranometer-interpolated data obtained from the calibration stations. From the 10 available validation stations, only 5 were chosen to perform this comparison. The criterion used was that they are evenly distributed in space and allow the division of Catalonia into three areas: north area (Girona station), central area (Montseny and Veciana stations), and south area (Benissanet and Deltebre stations).

The hourly global solar radiation from the calibration stations was interpolated into a grid with squares of

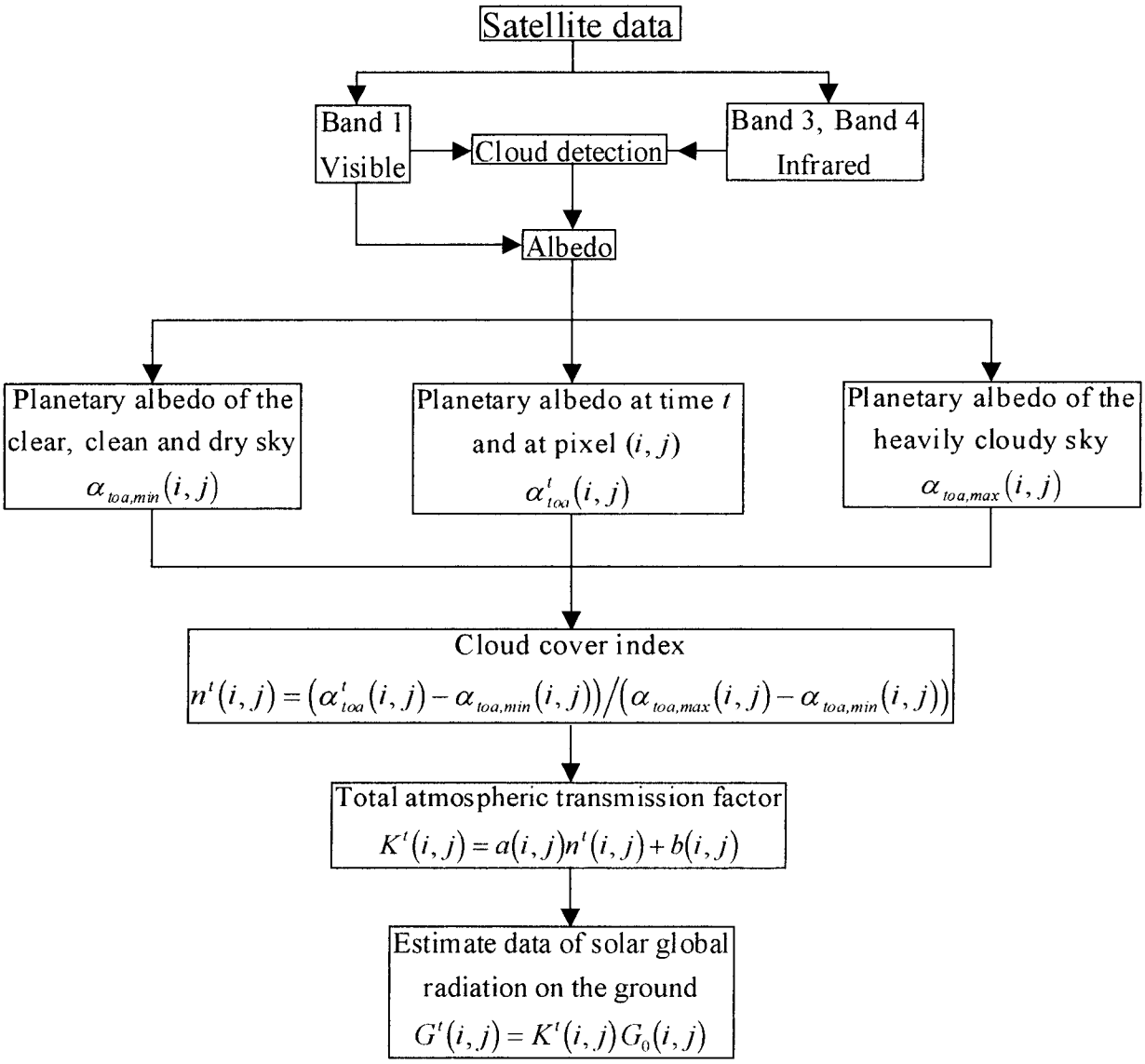


FIG. 4. Image-processing diagram.

dimension equal to that of the pixel provided by satellite images, using the kriging interpolation method, and applying the methodology described by Santabárbara et al. (1996) and Baldasano et al. (1999) for the elaboration of the *Solar Radiation Atlas of Catalonia* from the interpolation of surface pyranometer data.

The statistics of the comparison between satellite-estimated and surface-interpolated hourly global solar radiation at five validation stations in February and July of 1998 are shown in Table 5. The corresponding time series of the hourly global solar radiation is shown in Fig. 7.

Zelenka et al. (1999) considers that for any application requiring time/site-specific data, the user should rely on the satellite rather than on a neighboring ground station if the latter operates farther away than 20–30 km from the site. For the case of Catalonia, only in the north area (Girona station) are the ground measurement stations separated by more than 30 km. In that area, then, satellite-estimated values were more accurate (correlation of 0.90–0.96 and rmse of 6.9%) than were the surface-interpolated estimates (correlation of 0.75–0.79 and rmse of 11.4%–15.5%).

In the central area of Catalonia (Montseny and Veciana stations), the distance between the stations is almost that given in Zelenka's paper (1999). That is why satellite results (correlation of 0.91–0.97 and rmse of 3.2%–9.4%) are comparable to those obtained by surface interpolation (correlation of 0.74–0.87 and rmse of 4.1%–20.3%). However, it is evident that satellite-retrieved data are better because of the fact that the satellite takes into account spatial variations of the global

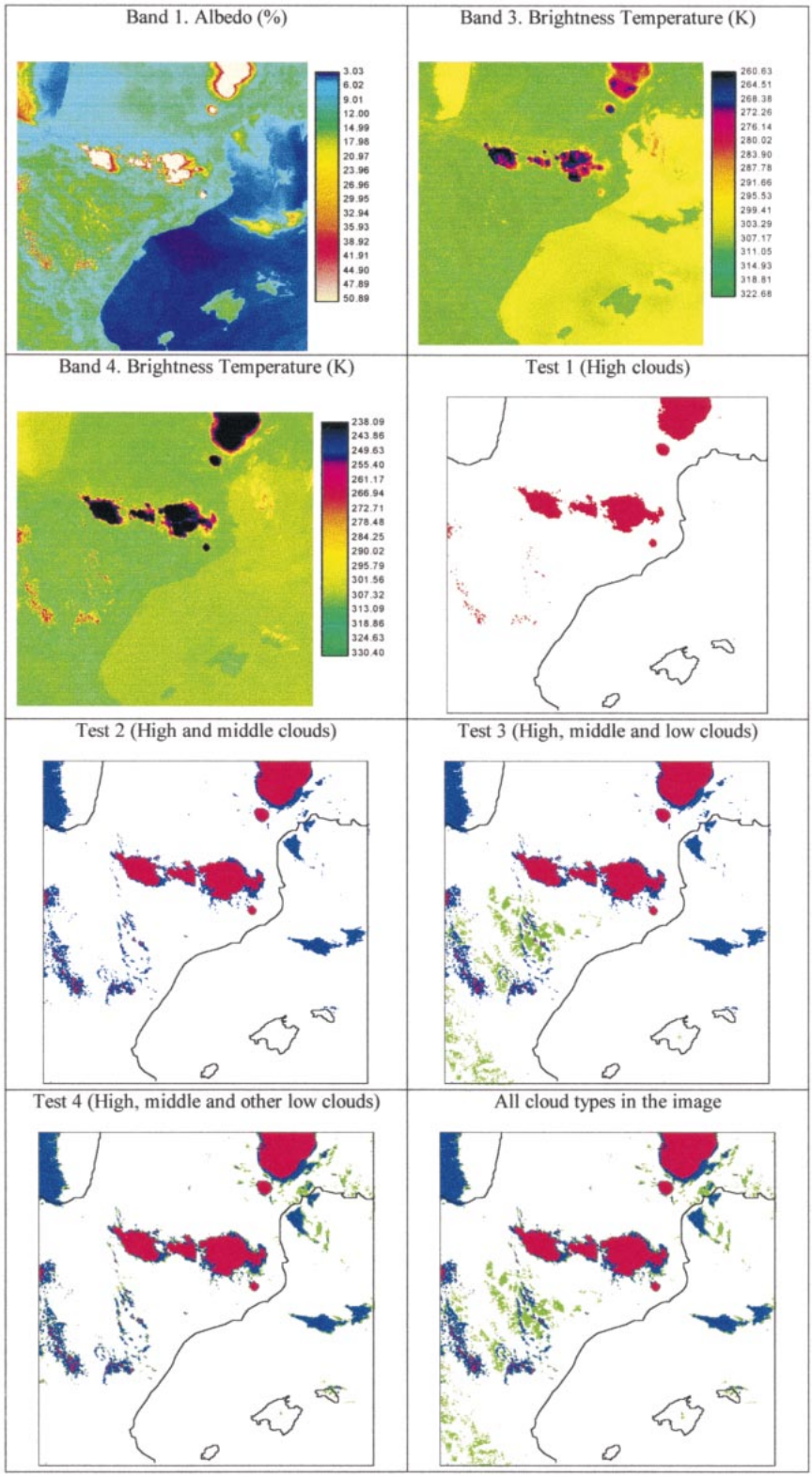


FIG. 5. An example of the cloud detection algorithm for a NOAA image corresponding to 11 Aug 1998.

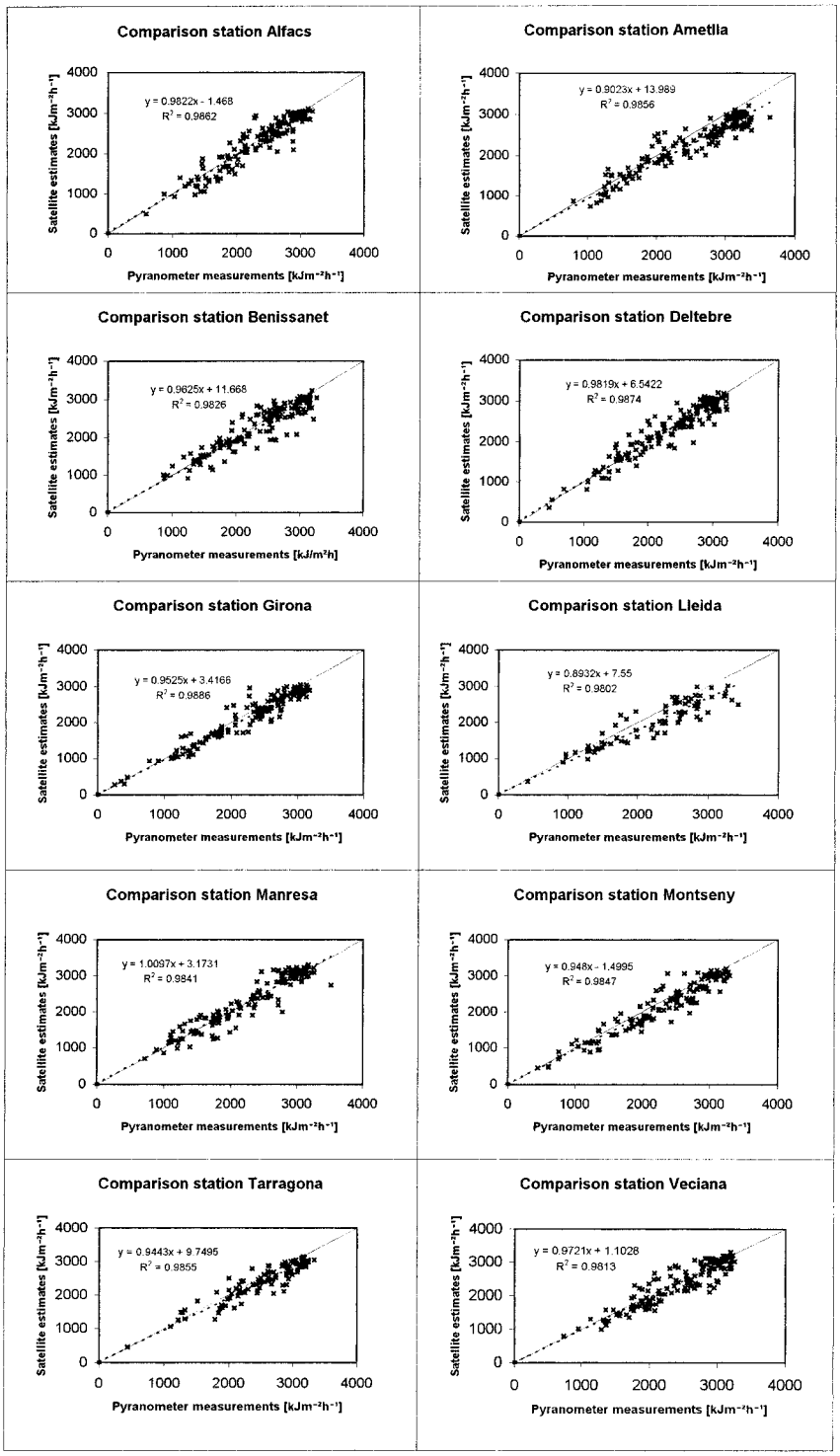


FIG. 6. Comparison between satellite-estimated and surface pyranometer-measured hourly global solar radiation for the period Feb–Dec 1998. The dotted line shows the regressions; the diagonal line (ratio 1:1) shows perfect agreement between pyranometer measurements and satellite estimates.

TABLE 4. Comparison of satellite estimates with hourly global solar radiation from ground measurement stations.

| Station | Determination coefficient $r^2$ | Mean (kJ m$^{-2}$ h$^{-1}$) | Rmse | | Bias | |
|---|---|---|---|---|---|---|
| | | | (kJ m$^{-2}$ h$^{-1}$) | (%) | (kJ m$^{-2}$ h$^{-1}$) | (%) |
| Alfacs | 0.986 | 2236.1 | 228.1 | 10.2 | −33.8 | −1.5 |
| Ametlla | 0.986 | 2572.5 | 407.3 | 15.8 | −175.5 | −6.8 |
| Benissanet | 0.983 | 2370.3 | 251.7 | 10.6 | −63.2 | −2.7 |
| Deltebre | 0.987 | 2400.4 | 231.0 | 9.6 | −18.4 | −0.8 |
| Girona | 0.989 | 2242.0 | 216.2 | 9.6 | −98.6 | −4.4 |
| Lleida | 0.980 | 2210.4 | 347.3 | 15.7 | −210.8 | −9.5 |
| Manresa | 0.984 | 2314.6 | 231.5 | 10.0 | 29.1 | 1.3 |
| Montseny | 0.985 | 2274.5 | 253.4 | 11.1 | −121.7 | −5.4 |
| Tarragona | 0.986 | 2541.8 | 251.0 | 9.9 | −123.0 | −4.8 |
| Veciana | 0.981 | 2480.1 | 284.4 | 11.5 | −57.5 | −2.3 |

radiation over the land whereas surface interpolation does not.

For the south area of Catalonia (Benissanet and Deltebre stations), results obtained from satellite (correlation of 0.93–0.97 and rmse of 5.3%–10.2%) and those from surface interpolation are of equal quality (correlation of 0.93–0.97 and rmse of 3.0%–14.6%).

Laine et al. (1999) undertook a similar analysis to check the accuracy of satellite and surface-interpolated estimates. The satellite-based daily global radiation spatial distributions were compared in the region of Finland with those obtained by interpolating the station-based pyranometer data. In southern Finland, the estimates of daily global radiation based on interpolated station data and based on satellite data were of equal quality (standard error of about 10%–15%). In northern Finland, where the stations are farther apart, the satellite-based values were much more accurate (standard error of 11%–16%) than were the interpolated estimates from the stations (standard error of 43%–74%).

Note that Laine et al. (1999) obtained larger differences between satellite estimates and surface-interpolated data in the north of Finland. This result is probably due to the low number of surface pyranometer stations and the nonhomogeneous distribution, with very low presence in the north. Catalonia, however has a very dense network of stations, although a little reduced in the north.

### c. Solar radiation map

Figure 8 shows the hourly global radiation as estimated by satellite between 1400 and 1500 LST for the period of February–December of 1998, and whenever possible the 15th of each month is represented. This day has been taken as the characteristic value for the specific month. All months were represented with the same value scale, so that they could be directly compared.

The map sequence of Fig. 8 clearly shows the seasonal variation of the surface global solar radiation, with minimum values occurring in December in agreement with the winter solstice. These values vary between 0.5 and 1.4 MJ m$^{-2}$ h$^{-1}$, and in space the minimum values are located in the Lleida plain, in the west of Catalonia, possibly because of the persistence of fog during the winter months. Other relative minima are located in the western area and the prelittoral mountain chain and in north Catalonia by the Pyrenean Mountains. The maximum values are found in June, coinciding with the absolute annual maxima and associated with the summer

TABLE 5. Comparison of satellite-estimated, surface pyranometer-interpolated, and pyranometer-measured hourly global solar radiation at five validation stations in Feb and Jul 1998.

| Station | Mean (kJ m$^{-2}$ h$^{-1}$) | Correlation | | Rmse | | | |
|---|---|---|---|---|---|---|---|
| | | Satellite $r$ | Interpolation $r$ | Satellite | | Interpolation | |
| | | | | (kJ m$^{-2}$ h$^{-1}$) | (%) | (kJ m$^{-2}$ h$^{-1}$) | (%) |
| | | | Feb | | | | |
| Girona | 1684.4 | 0.96 | 0.75 | 115.9 | 6.9 | 260.8 | 15.5 |
| Montseny | 1839.9 | 0.97 | 0.76 | 172.5 | 9.4 | 373.4 | 20.3 |
| Veciana | 1984.9 | 0.96 | 0.87 | 141.5 | 7.1 | 277.4 | 14.0 |
| Benissanet | 1747.6 | 0.95 | 0.97 | 178.1 | 10.2 | 255.4 | 14.6 |
| Deltebre | 1779.6 | 0.97 | 0.94 | 94.3 | 5.3 | 159.2 | 9.0 |
| | | | Jul | | | | |
| Girona | 2722.2 | 0.90 | 0.79 | 188.0 | 6.9 | 311.0 | 11.4 |
| Montseny | 2797.3 | 0.94 | 0.74 | 146.2 | 5.2 | 274.5 | 9.8 |
| Veciana | 3026.5 | 0.91 | 0.74 | 96.4 | 3.2 | 124.0 | 4.1 |
| Benissanet | 2843.5 | 0.93 | 0.93 | 174.6 | 6.1 | 190.5 | 6.7 |
| Deltebre | 2799.1 | 0.95 | 0.99 | 169.6 | 6.1 | 83.8 | 3.0 |

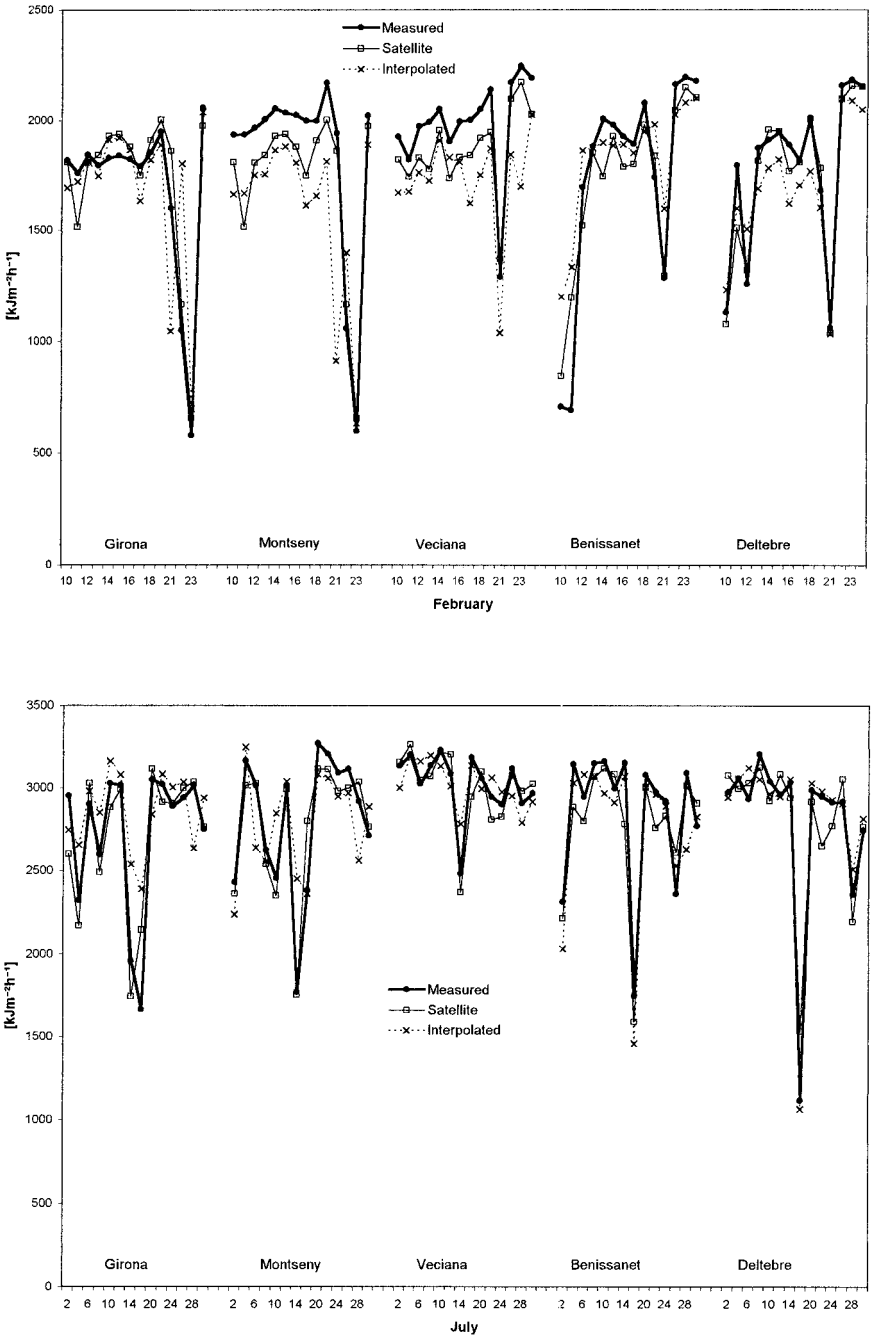


FIG. 7. Time series of the comparison of satellite-estimated, surface pyranometer-interpolated, and pyranometer-measured hourly global solar radiation at five validation stations in Feb and Jul 1998.

solstice, with values around 3.4 MJ $m^{-2}$ $h^{-1}$. For the spatial distribution, maximum values are registered at the coast and in the western central area of Catalonia, with a slight reduction in the precoastal strip and certain minima in the Girona Pyrenean Mountains to the northeast of Catalonia. Values for the Pyrenees are very variable in a small region, but this variability is due to the characteristics of the measurement points. It is clear that mountain stations, with a good exposure to the sun and less optical mass, record high average values, whereas the low-level stations show lower average values.

## 5. Conclusions

In this paper, a statistical model is applied in the determination of hourly global solar radiation, employ-

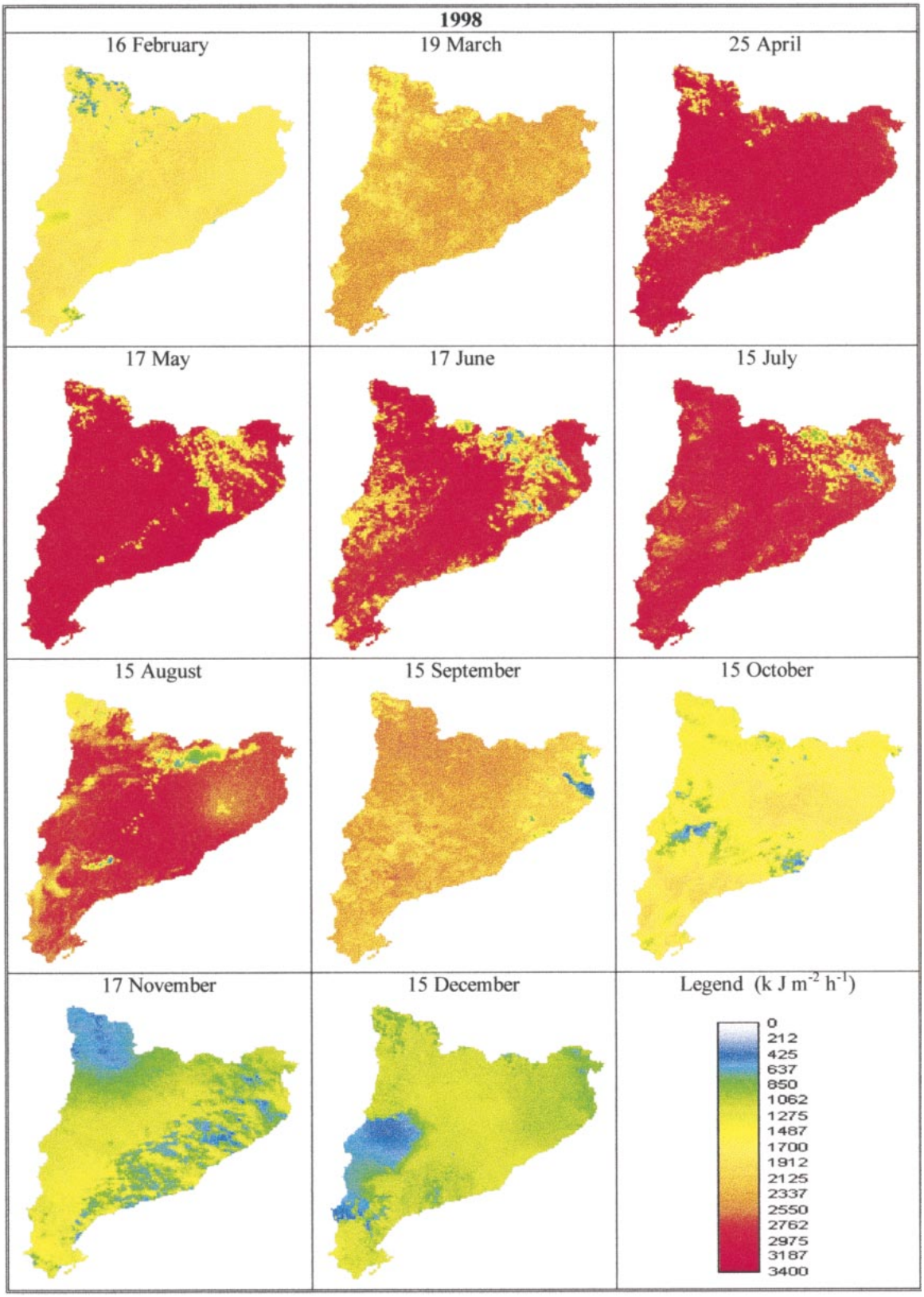


FIG. 8. Map of the hourly global radiation estimated between 1400 and 1500 LST.

ing NOAA AVHRR satellite data. The model coefficients were determined from the data provided by 11 ground measurement stations, obtaining high coefficients of determination (with a mean value of about 0.80) for the regression model. For the model's coefficients, the coefficient $b$ represents the transmission with a clear sky, with a mean value of around 0.76, and it was seen that it was much more stable than the coefficient $a$, which represents the slope of the curve, which was highly influenced by cloud conditions, with a variation of between $-0.86$ and $-0.07$ and a mean slope of $-0.49$.

Once the regression coefficients were obtained, they were applied to the statistical model. The model's results were validated by comparing them with the data coming from 10 ground measurement stations that were independent of those employed in the determination of the coefficients, obtaining model estimates that fitted very well with the measurements, with a determination coefficient of $r^2$ greater than 0.98 in all cases, together with an rmse that varied between 9.6% and 15.8% and a bias of $-9.5\%$ to 1.3%.

The satellite-estimated hourly global solar radiation values were compared with those obtained by surface-interpolated pyranometer and with measured pyranometer data at five validation stations: Girona, Montseny, Veciana, Benissanet, and Deltebre.

In southern Catalonia, the satellite estimation and the surface-interpolated data were of equal quality (rmse of about 3%–15%). In northern Catalonia, where the stations have a larger separation, the satellite-estimated values were more accurate (rmse of 7%) than those interpolated from stations (rmse of 11%–16%).

The satellite-based method offers more exact spatial estimates for hourly global radiation than do the interpolated estimates based on station measurements, especially in regions for which the stations network is sparse. For cloud detection, a simple thresholding scheme with the AVHRR channel was used. According to a visual check of the efficiency for the separation of clouds and snow, values of close 100% were obtained under snow-free conditions. These results clearly demonstrate that satellite data can be used successfully for mapping both the global radiation at ground level and the cloud coverage over large areas, with a ground resolution around 1.1 km $\times$ 1.1 km. This technique may be employed to obtain detailed solar radiation maps for various years of surface measurement records and satellite data, which are highly appreciated by scientists, engineers, and users within the solar energy field, both for the evaluation and dimensioning of buildings with solar technology, and for its use in agriculture and meteorology.

*Acknowledgments.* This paper was made possible thanks to the MUTIS grant from the Spanish government and the European Union ALFA program. The authors also thank Dr. Jordi Cunillera from the Department for the Environment of the Generalitat of Catalonia for kindly providing the satellite images and other information that was used in the preparation of this paper. We acknowledge the useful comments of anonymous referees, which have substantially improved this paper.

## REFERENCES

Allen, R., P. Durkee, and C. H. Wash, 1990: Snow/cloud discrimination with multispectral satellite measurements. *J. Appl. Meteor.,* **29,** 994–1004.

Baldasano, J. M., C. Soriano, and H. Flores, 1999: *Atlas de Radiació Solar a Catalunya (Dades del període 1964–1997)* [Solar Radiation Atlas of Catalonia (For the period of 1964–1997)]. Institut Catalá d'Energia, 71 pp.

Beyer, H. G., G. Czeplak, U. Terzenbach, and L. Wald, 1997: Assessment of the method used to construct clearness index maps for the new European Solar Radiation Atlas (ESRA). *Sol. Energy,* **61,** 389–397.

Bishop, J. K. B., W. B. Rossow, and E. G. Dutton, 1997: Surface solar irradiance from the International Satellite Cloud Climatology Project: 1983–1991. *J. Geophys. Res.,* **102,** 6883–6910.

Cano, D., J. M. Monget, M. Albuisson, H. Guillard, N. Regas, and L. Wald, 1986: A method for the determination of the solar radiation from meteorological satellite data. *Sol. Energy,* **37,** 31–39.

Diabaté, L., G. Moussu, and L. Wald, 1989: Description of an operational tool for determining global solar radiation at ground using geostationary satellite images. *Sol. Energy,* **42,** 201–207.

Gautier, C., G. Diak, and S. Masse, 1980: A simple physical model to estimate incident solar radiation at the surface from GOES satellite data. *J. Appl. Meteor.,* **19,** 1005–1012.

Karlsson, K. G., 1989: Development of an operational cloud classification model. *Int. J. Remote Sens.,* **10,** 687–693.

Kasten, F., H. J. Golchert, R. Dogniaux, and M. Lemoine, 1996: *European Solar Radiation Atlas*. W. Palz and J. Greif, Eds., 3d ed., Springer-Verlag, 333 pp.

Laine, V., A. Venäläinen, M. Heikinheimo, and O. Hyvärinen, 1999: Estimation of surface solar global radiation from NOAA AVHRR data in high latitudes. *J. Appl. Meteor.*, **38,** 1706–1719.

Noia, M., C. Ratto, and R. Festa, 1993: Solar irradiance estimation from geostationary satellite data. Part I: Statistical models. *Sol. Energy,* **51,** 465–499.

Nunez, M., 1987: A satellite-based solar energy monitoring system for Tasmania, Australia. *Sol. Energy,* **39,** 439–444.

Pinker, R. T., R. Frouin, and Z. Li, 1995: A review of satellite methods to derive surface shortwave irradiance. *Remote Sens. Environ.,* **51,** 108–124.

Rafiqul, I. M. D., and H. B. Exell, 1996: Solar radiation mapping from satellite image using a low cost system. *Sol. Energy,* **56,** 225–237.

Santabárbara, J. M., J. Calbó, J. M. Baldasano, J. Esteve, and A. Mitja, 1996: Month to month variation of global solar radiation in Catalonia, Spain. *Int. J. Climatol.,* **16,** 711–721.

Tarpley, J. D., 1979: Estimating incident solar radiation at the surface from geostationary satellite data. *J. Appl. Meteor.,* **18,** 1172–1181.

Zelenka, A., R. Perez, R. Seals, and D. Renné, 1999: Effective accuracy of satellite-derived hourly irradiances. *Theor. Appl. Climatol.,* **62,** 199–207.